Chen, C., Lin, C.-H., Wei, D., and Chen, Q. 2016. "Modeling particle deposition on the surfaces around a multi-slot diffuser," *Building and Environment*, 107: 79-89.

Modeling Particle Deposition on the Surfaces around a Multi-Slot Diffuser

Chun Chen[1,2], Chao-Hsin Lin[3], Daniel Wei[4], and Qingyan Chen[1,5*]

[1] School of Mechanical Engineering, Purdue University, West Lafayette, IN 47907, USA
[2] Department of Mechanical and Automation Engineering, The Chinese University of Hong Kong, Shatin, N.T. 999077, Hong Kong SAR, China
[3] Environmental Control Systems, Boeing Commercial Airplanes, Everett, WA 98203, USA
[4] Boeing Research & Technology, Beijing 100027, China
[5] School of Environmental Science and Engineering, Tianjin University, Tianjin 300072, China

[*] Phone: (765) 496-7562, Fax: (765) 496-0539, Email: yanchen@purdue.edu

Abstract

Enhanced soiling on the wall/ceiling around a diffuser due to particle deposition is very unsightly and reduces our quality of life. This study aimed to model the particle deposition on the surfaces around multi-slot diffusers, which are widely used in transportation vehicles. An SST k-ω model with a modified Lagrangian method was proposed and validated with experimental data on particle deposition rate from the literature. This investigation then conducted chamber tests to qualitatively validate model's ability to predict the deposition distribution around a multi-slot diffuser. Using the validated model, this study numerically investigated the effects of slot setting, supply air angle, and temperature differential on particle deposition around a multi-slot diffuser. The results indicated that, with the same supply airflow rate, increasing the area ratio of openings to bars in a multi-slot diffuser can reduce the particle deposition. When the angle between the supply air jet and the wall was increased to more than 45°, the particle deposition was significantly reduced. Furthermore, the impact of thermophoresis on particle deposition around a multi-slot diffuser was negligible.

Keywords: Indoor environment; Computational fluid dynamics (CFD); Aerosol; Lagrangian tracking; Black magic dust; Soiling.

1. Introduction

There is strong evidence of a relationship between exposure to ambient particles and adverse health effects, such as lung cancer [1], asthma [2], and mortality [3]. However, a large amount of ambient particles can penetrate through cracks in building envelopes into indoor spaces [4], where people spend roughly 90% of their time [5]. Thus, exposure to indoor particles has become a major threat to public health [6]. These particles deposit onto indoor surfaces, with mixed effects on our daily lives. On one hand, particle deposition reduces indoor exposure to airborne particles [7,8]. On the other hand, particle deposition can cause discoloration of and damage to indoor surfaces [9,10]. Such significant impacts on our health and environment have driven the rapid development of research on indoor particle deposition.

Numerous experimental and modeling studies have focused on quantifying particle deposition indoors. A comprehensive review by Lai [7] systematically summarized the experimental data on particle deposition rates that was published before 2002. Generally speaking, higher deposition rates were observed for both ultrafine (<0.1 μm) and coarse (>1 μm) particles than for accumulation mode particles (0.1 to 1 μm). This difference occurred because Brownian and turbulent diffusion were dominant for ultrafine particles, and gravitational settling for coarse particles, whereas neither of these mechanisms was dominant for accumulation mode particles. Most of the measured particle deposition rates published after 2002 have shown a similar "V-shape" trend [11-17].

In addition to experimental studies, many efforts have been made to model indoor particle deposition. Eulerian and Lagrangian modeling are the most popular methods to be adopted for indoor environments. The Eulerian method solves the equation that describes the particle flux through the boundary layer to a certain surface. Lai and Nazaroff [18] developed a semi-empirical Eulerian deposition model by considering the effects of Brownian and turbulent diffusion and gravitational settling. Building on Lai and Nazaroff's model, Zhao and Wu [19] considered the effect of thermophoresis. To account for the effects of airflow and turbulence distribution indoors, a number of researchers have implemented the Eulerian deposition models into computational fluid dynamics (CFD) codes [20-23]. Other influencing factors, such as the thermophoretic, lift, and electrostatic forces, have also been investigated using the Eulerian method [24,25]. On the other hand, many studies have calculated indoor particle deposition by means of the Lagrangian method [26-29]. The Lagrangian method tracks the trajectory of each particle, usually on the basis of the airflow distribution calculated from CFD. When particle resuspension is negligible, the trajectory calculations are terminated as a particle deposits onto a surface. Integrating CFD into the calculation allows the distribution of particle deposition to be obtained. For instance, Wang et al. [29] quantified the deposition of exhaled infectious particles onto passengers, floor, ceiling, walls, seat backs, and tray tables in an aircraft cabin. This information is essential for assessing the risk of infection through indirect contact.

Most of the studies mentioned above quantified particle deposition in order to accurately evaluate indoor exposure to airborne particles. However, particle deposition can also increase the soiling of indoor surfaces, a phenomenon which has not been thoroughly investigated. This enhanced soiling has been referred as "black magic dust" in several other studies [10,30]. The soiling usually appears on the wall above a heater, the wall/ceiling around a diffuser, the ceiling above a lamp, and/or the corners of walls/ceiling in a few weeks to a few months after the system is in operation. Many factors have been found to be correlated with this phenomenon,

including elevated concentrations of particulate matter ($PM_{2.5}$ and PM_{10}) and semi-volatile organic compounds (SVOCs), a large temperature differential, local airflow characteristics, and a low air exchange rate [10,30]. A possible pathway for the deposition of the stains is that the gaseous SVOCs condense on airborne particles, and they deposit together onto the surfaces [30]. Elevated particle and SVOC concentrations, which are frequently correlated with a low air exchange rate [31], would lead to an increased amount of deposited particles [30]. Chen and colleagues investigated particle deposition above a heater next to a wall, both experimentally [32] and numerically [33]. It was found that a larger temperature differential between the wall and the heater increased the amount of deposited particles. Timmer and Zeller [34] performed CFD simulation with a Lagrangian method to calculate the particle deposition around a ceiling induction outlet. They found that local airflow characteristics were the decisive factors in particle deposition.

Although these studies have provided great insight into enhanced soiling indoors, the understanding of this phenomenon is still far from complete. One case is that of soiling on the wall/ceiling around a diffuser, which is frequently observed in indoor environments [35,36]. Although the soiling around a diffuser is very unsightly and reduces our quality of life, there is a lack of scientific literature on this issue. Multi-slot diffusers are widely used in transportation vehicles, such as aircraft cabins, in order to meet air distribution specifications [37-39]. The enhanced soiling on the wall/ceiling around these diffusers could be a problem. To increase the body of knowledge in this field, the present study aimed to model the particle deposition around a multi-slot diffuser using a CFD technique with Lagrangian tracking. The proposed model was validated by experimental deposition-rate data from the literature. This investigation also conducted chamber tests to qualitatively validate the model's ability to predict particle deposition distribution around a slot diffuser. Finally, the effects of slot setting, supply air angle, and temperature differential on particle deposition were numerically evaluated. The results could be used in the design of multi-slot diffusers in order to prevent enhanced soiling.

2. Methods

2.1 Airflow and turbulence model

This investigation used the shear stress transport (SST) k-ω model [40] to calculate the indoor airflow field. The SST k-ω model uses a transformed standard k-ε model in the free shear region and the standard k-ω model in the near-wall region. This model not only directly resolves the airflow in the near-wall region, but also enhances the robustness in predicting the mean velocity of free shear flows in the wake region [40]. Previous comparative studies concluded that the SST k-ω model was the most effective model for predicting a jet flow [41,42]. Since the airflow from a diffuser slot is a jet in nature, the SST model was utilized in the present study to calculate the airflow field.

2.2 Particle motion and deposition model

This study followed the Lagrangian method to calculate the trajectory of each particle, using the momentum equation based on Newton's law:

$$\frac{d\vec{u}_p}{dt} = F_D(\vec{u}_a - \vec{u}_p) + \frac{\vec{g}(\rho_p - \rho_a)}{\rho_p} + \vec{F} \quad (1)$$

where t is the time, $\vec{u}_p$ the particle velocity, $\vec{u}_a$ the air velocity, $\vec{g}$ the gravitational

acceleration, ρ_p and ρ_a the particle and air density, respectively, and $\vec{F}$ the Brownian motion and thermophoretic force. The drag force, $F_D(\vec{u}_a - \vec{u}_p)$, can be calculated by:

$$F_D(\vec{u}_a - \vec{u}_p) = \frac{18\mu_a}{\rho_p d_p^2 C_c}(\vec{u}_a - \vec{u}_p) \quad (2)$$

where μ_α is the air viscosity, d_p the particle diameter, Re the Reynolds number, and C_c the Cunningham correction to Stokes' drag law, which can be calculated by:

$$C_c = 1 + \frac{\lambda}{d_p}(2.514 + 0.8\exp(-0.55\frac{d_p}{\lambda})) \quad (3)$$

where λ is the mean free path of air molecules. This investigation used the discrete random walk (DRW) model to calculate the turbulence dispersion:

$$u'_i = \zeta_i\sqrt{2k/3} \quad (4)$$

where u'_i is turbulent fluctuating air velocity, ζ_i a standard normal random number, and k the turbulence kinetic energy. This study assumed the particle resuspension to be negligible, since the particles usually cannot accumulate enough rebound energy to overcome the adhesion force [43,44]. Thus, when a particle reaches a surface, the calculation of particle trajectory is terminated, and the particle is considered to have deposited onto the surface. This study also assumed that all the surfaces were smooth.

For turbulent dispersion within a turbulent boundary layer, particles are driven to the wall by the turbulent fluctuating velocity component in the direction normal to the wall. In the near-wall region, the turbulent fluctuating velocity in the wall-normal direction is smaller than that parallel to the wall. However, the SST k-ω model assumes the turbulence to be isotropic, which over-predicts the fluctuating velocity in the wall-normal direction. Consequently, the particle deposition will also be over-predicted [45]. Many studies have adopted near-wall corrections to the fluctuating velocity component in the direction normal to the wall, which could improve the prediction of particle deposition [27,29,46,47]. Wang and James [48] proposed damping functions for the fluctuating velocity components in the near-wall region by assuming that the ratios of the three Reynolds stress components to the turbulent kinetic energy were fixed. The functions were developed by curve fitting the direct numerical simulation (DNS) data from Kim et al. [49], which is valid for dimensionless wall distances, y^+, less than 80. Matida et al. [46] then used the damping function for the fluctuating velocity component in the direction normal to the wall to modify the turbulence kinetic energy for the near-wall cells, which significantly improved the prediction of particle deposition. However, the fixed-ratio assumption of the damping functions developed by Wang and James [48] was not justified by theoretical derivation, as pointed out by Lai and Chen [27]. Thus, Lai and Chen [27] used the damping function derived theoretically by He and Ahmadi [50] to modify the turbulence kinetic energy in near-wall cells. This damping function is valid only for y+ values less than 2.5 [28]. To take advantage of the findings in both studies mentioned above, the present study proposed the following damping function to modify the turbulence kinetic energy for the near-wall cells:

$$k_{near\_wall} = \begin{cases} \frac{3}{2}[u^*(0.008y^{+^2})]^2 & y^+ \le 2.5 \\ \frac{3}{2}[u^*(0.0000029y^{+^3} - 0.000616y^{+^2} + 0.0412y^+ - 0.042)^2]^2 & 2.5 < y^+ \le 80 \end{cases} \quad (5)$$

where u^* is the friction velocity and y^+ the dimensionless wall distance. The damping function for y^+ values less than 2.5 was that proposed by Lai and Chen [27], which was justified by theoretical derivation. The function for y^+ values from 2.5 to 80 was developed by curve fitting the DNS data from Kim et al. [49] with a R^2 of 0.99. Note that the modified turbulence kinetic energy for the near-wall cells remains isotropic, but the fluctuating velocity in the wall-normal direction can be correctly predicted. Although the fluctuating velocity in the direction parallel to the wall would be under-estimated, the impact of this drawback is minimal. This is because the particle motion in the direction parallel to the wall depends more on the mean velocity than on the fluctuating velocity [27,46].

When the modified near-wall turbulence kinetic energy has been determined, the particle deposition velocity can be accurately calculated. Most of the existing studies calculated the overall deposition velocity for a wall, ceiling, floor, or entire room [7]. However, there are specific patterns to the enhanced soiling around a diffuser due to particle deposition [36]. To better understand the process of particle deposition on the wall/ceiling around a multi-slot diffuser, the detailed distribution of deposited particles should be obtained. Therefore, this study calculated the local particle deposition velocity for each of the computing meshes used on the surfaces. Initially, a certain amount of particles was evenly released into the space. The proposed model was then used to calculate the particle motion and deposition. For a given computing mesh on a surface, i, the local particle deposition velocity can be calculated by [28]:

$$v_{d,i} = \frac{N_{d,i}/(A_i \cdot t)}{\bar{N}/V} \quad (6)$$

where t is the time, A_i the area of the local computing mesh, $N_{d,i}$ the number of particles depositing onto this mesh within t, $\bar{N}$ the averaged number of particles in the indoor space within t, and V the volume of the space. This study tested the influence of time on the calculation of particle deposition velocity. It was found that a time ranging from 1 to 4 room time constants could obtain consistent and accurate results. Note that the denominator of Eq. (6) is the averaged particle concentration for the indoor space (C_{indoor}), instead of the particle concentration outside the concentration boundary layer (normally denoted as C_∞). The reason of using C_{indoor} instead of C_∞ as the reference will be discussed after Eq. (7).

In the heating, ventilation, and air-conditioning (HVAC) industry, the particle accumulation per square meter, expressed in g/m^2, is widely used to evaluate the cleanliness of a surface. For instance, the North American Duct Cleaners Association (NADCA) requires that the amount of residual dust in ducts after cleaning not exceed 0.1 g/m^2 [51]. The Heating and Ventilating Contractors' Association (HVCA) in the UK has set the limit for dust accumulation at 1.0 g/m^2 for supply air ducts [52]. The same limit has been specified in one of the cleanliness categories of the Finnish indoor climate guidelines [53]. Holopainen et al. [54] conducted a subject study of a visual inspection method for evaluating the cleanliness of air ducts. It was found that, when

the particle accumulation was less than 0.1 g/m^2, the stains were almost invisible. However, when the accumulation was greater than 1.0 g/m^2, the stains could be easily observed by professional cleanliness inspectors. The particle accumulation at a given computing mesh on a surface over a certain period of HVAC system operation can be calculated by:

$$m_i = v_{d,i} C_{indoor} t^* \tag{7}$$

where C_{indoor} is the averaged particle concentration indoors, and t^* the period of HVAC system operation. Note that, if C_∞ is used as the reference in Eq. (6), the C_{indoor} in Eq. (7) should be replaced by C_∞ as well. In that case, one should extract the information of C_∞ for each surface, which could be time-consuming. Thus, although the calculated local particle accumulations are the same, using C_{indoor} instead of C_∞ is more convenient for calculating the local particle accumulation.

The airflow field and particle trajectories were calculated using the CFD code ANSYS Fluent 16.0 [55]. User-defined functions were implemented in order to (1) record the amount of particles depositing onto each computing mesh of the surfaces, (2) convert the Lagrangian trajectory information to the form of particle number concentrations, and (3) calculate the local deposition velocity for each computing mesh on the surfaces and the particle accumulations.

3. Validation

Most of the previous experimental studies were only able to measure the overall particle deposition rates for the whole indoor space [7]. Thus, the present study first used two sets of measured overall particle deposition rates from the literature to quantitatively validate the proposed model. Since the study aimed to calculate the particle deposition on the wall/ceiling around a multi-slot diffuser, obtaining the detailed distribution of deposition was crucial. To our best knowledge, no experimental data was available for the distribution of particle deposition on a surface near a multi-slot diffuser. Therefore, this investigation conducted chamber tests to visualize this distribution. The experimental results were used to qualitatively validate the model's ability to predict particle deposition distribution.

3.1 Quantitative validation for particle deposition rate

This investigation first used two cases of indoor particle deposition with experimental data from the literature [26,56] to quantitatively validate the proposed model. In both studies, the overall particle deposition rate, expressed in 1/s, was measured using the particle decay method. The overall particle deposition rate can be calculated on the basis of the deposition velocities calculated from Eq. (6):

$$K = \frac{\sum_{i=1}^{n} (v_{d,i} \cdot A_i)}{V} \tag{8}$$

Another method for calculating the overall particle deposition rate is the decay method, which is analogous to the method normally used in experiments. First, the decay curve of the space-averaged particle concentration is calculated as a function of time. The deposition rate can then be obtained through regression analysis according to the following equation:

$$C(t) = C(0)\, e^{-(a+K)t} \tag{9}$$

where C(t) is the space-averaged particle concentration at time t, C(0) the initial concentration, and a the air change rate. This study used both methods to calculate the overall deposition rate and compared the results with the experimental data.

3.1.1 Particle deposition in a ventilated chamber

The first case was the deposition of particles in a ventilated chamber under isothermal conditions, as studied by Bouilly et al. [26]. The chamber had dimensions of 2.5 x 2.5 x 2.5 m^3. As shown in Figure 1, the ventilation system supplied air from the inlet located in the left-hand wall near the ceiling, and the exhaust was installed in the right-hand wall near the floor. The sizes of the inlet and exhaust openings were the same (0.07 x 0.07 m^2). The supply air velocity was 0.44 m/s, which corresponds to an air change rate of 0.5 ACH. The particle diameters ranged from 0.3 to 15 μm.

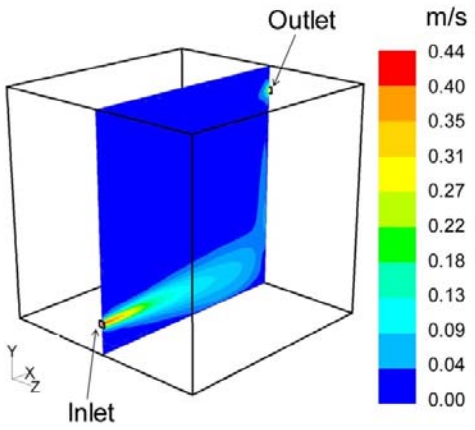

Figure 1. Configuration and airflow pattern of the chamber studied by Bouilly et al. [26].

Three grid resolutions (134,234, 324,386, and 1,234,090) were tested for CFD grid independence. It was found that a grid number of 324,386 was sufficiently fine to capture the turbulence in the chamber. The calculated airflow pattern is shown in Figure 1. Before the particle calculations were performed, the turbulence kinetic energy in the near-wall cells was modified using Eq. (5). This investigation then released 0.064, 0.125, and 0.343 million particles, respectively, evenly with a certain diameter into the chamber and calculated the motion and deposition of the particles by Lagrangian tracking. It was found that 0.125 million particles were sufficient to obtain particle number independent results. The calculations were repeated for a total of 11 particle sizes ranging from 0.1 to 15 μm. The overall particle deposition rates were calculated using the two methods (Eqs. (8) and (9)) in order to cross check the calculations. The mean relative difference between the calculated deposition rates from these two methods was only 2.6%. Thus, both methods could be utilized. This study used the results calculated by Eq. (8) for comparison with the experimental data.

Figure 2 compares the predicted particle deposition rates with the measured data from Bouilly et al. [26]. The proposed model correctly predicted the relatively low deposition rates for particles with diameters from 0.3 to 1 μm. The increase in particle deposition rate with the increase in particle size from 1 to 15 μm was also correctly predicted. All of the calculated deposition rates were within the error bars of the measured data. Thus, in general, the proposed model can accurately predict the particle deposition for this chamber.

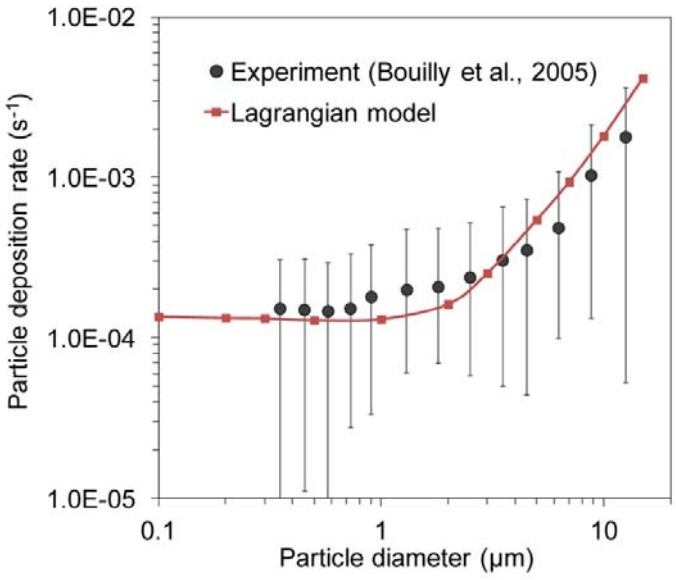

Figure 2. Comparison of the predicted particle deposition rate with measured data from Bouilly et al. [26].

3.1.2 Particle deposition in a sealed chamber with a mixing fan

The second case was that of particle deposition in a sealed chamber with a mixing fan, as shown in Figure 3, studied by You et al. [56]. The chamber had dimensions of 2 x 2 x 2 m^3. The air change rate of the chamber was lower than 0.01 ACH, which means that the chamber was airtight. The temperature in the chamber was controlled at a constant value. The deposition rates of particles with diameters ranging from 0.3 to 10 μm were measured using the decay method.

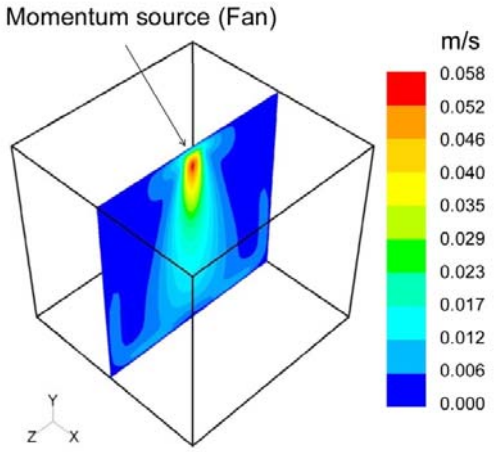

Figure 3. Configuration and airflow pattern of the chamber studied by You et al. [56].

Our simulation used a momentum source to model the mixing fan, as proposed by Bredell et al. [57]. Three grid resolutions (27,000, 64,000, and 216,000) were tested, and a grid number of 64,000 was found to provide grid-independent results. The airflow pattern is shown in Figure 3. The predicted air velocity matched the measured data at a distance of 0.5 m below the fan. After the turbulence kinetic energy had been modified in near-wall cells and a particle number

independence test had been conducted, 0.125 million particles of a given size were evenly released into the chamber. The particle motion and deposition were calculated using the proposed model. The particle calculations were repeated for a total of 10 particle sizes from 0.1 to 10 μm. This study again calculated the deposition rates using both Eqs. (8) and (9). The mean relative difference between these two methods was only 4.1%. The results calculated by Eq. (8) were then used for comparison with the experimental data.

Figure 4 compares the predicted particle deposition rates with the measured data for this case. The numerical model provided a good prediction of the particle deposition rates in this chamber, expect for the particles with a diameter of 0.4 μm. The measured deposition rate for particles of this size was 0.013 per hour, which is on the same order of magnitude as the air change rate due to leakage. The measured data did not account for the effect of leakage, which may explain the inconsistency at this point. Generally speaking, the proposed model can predict the indoor particle deposition reasonably well.

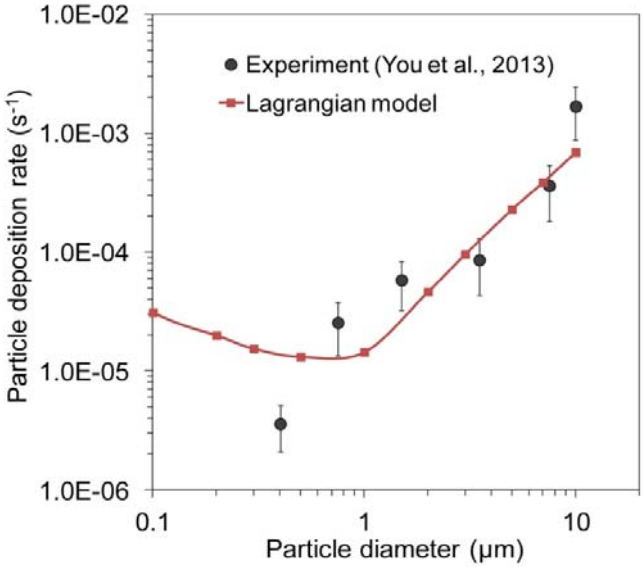

Figure 4. Comparison of the predicted particle deposition rate with measured data from You et al. [56].

3.2 Qualitative validation for particle deposition distribution

In addition to the quantitative validation above, this study conducted chamber tests to qualitatively validate the model's ability to predict particle deposition distribution.

3.2.1 Experimental setup

This study used a chamber with dimensions of 1.75, 0.9, and 2.2 m in the x, y, and z directions, respectively, as shown in Figure 5(a). The inlets were installed at ceiling level next to the left-hand wall. Two diffusers, a multi-slot diffuser and a linear diffuser as shown in Figure 5(b), with the same length (0.45 m in the y direction), were used for comparison. The width of each diffuser was 0.02 m (in the x direction). The length of each opening was 0.05 m, and that of each of the bars between the openings was also 0.05 m. The exhaust was located on the right-hand wall at floor level. A solid box was placed inside the chamber. A high-efficiency particulate arrestance (HEPA) filter was installed in the ventilation system to minimize the

particle concentration at the inlet. The supply air velocity was 1.99 m/s, and the supply air direction was parallel to the left-hand wall. The temperature inside the chamber was controlled at 24 °C.

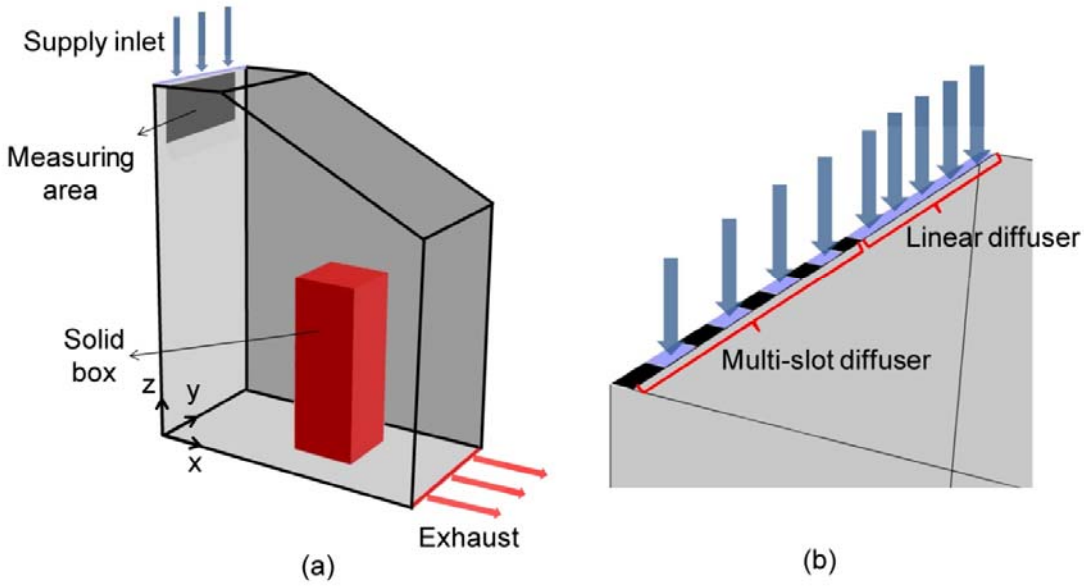

Figure 5. (a) The chamber configuration and (b) the air supply by means of a multi-slot diffuser (left) and a linear diffuser (right).

Arizona test dust, consisting of $PM_{2.5}$ and PM_{10}, was used to simulate particulate contaminants indoors. Figure 6 shows the size distributions of the $PM_{2.5}$ and PM_{10} used in this study. The representative sizes for the $PM_{2.5}$ and PM_{10} were 1 and 5 μm, respectively. To obtain good visualization of the deposited particles, this study used black cardstock paper to cover the upper part of the left-hand wall directly under the diffusers, as shown in Figure 5(a). Before the start of each test, the ventilation system was operated for half an hour to achieve a stable air distribution. Next, 15 g of test particles were released into the chamber using a particle injector. Within 10 minutes (approximately 5 room time constants), all the particles were either removed through the exhaust or deposited onto the surfaces. Photographs of the cardstock paper with the deposited particles were then taken in order to obtain information about the particle deposition distribution. The tests for both $PM_{2.5}$ and PM_{10} were performed more than once, to ensure repeatability. For observation of the particle deposition pattern within a short period of time, much higher particle concentrations were generated in this study than would be found in normal indoor environments. However, the experiment was still meaningful because the aim was to provide qualitative information about the particle deposition pattern for validation of the proposed model.

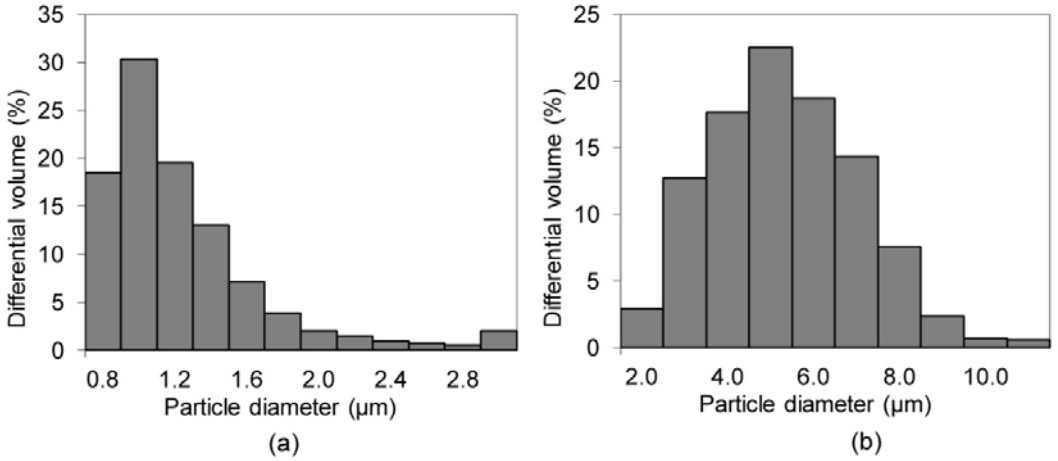

Figure 6. Size distribution of test particles: (a) $PM_{2.5}$ and (b) PM_{10}.

The multi-slot diffuser in the tests above supplied air parallel to the left-hand wall. To obtain additional experimental results for model validation, this study also installed a multi-slot diffuser that supplied air at an angle of 45° between the jets and the left-hand wall. This diffuser had 49 slots. The length of each opening was 9.2 mm, and that of each of the bars between the openings was 2.1 mm. The width of the diffuser was 5.7 mm. The total supply airflow rate was 0.013 m^3/s. The particle deposition distribution was again obtained using the method described above.

3.2.2 Qualitative validation

This investigation used the proposed model to calculate the particle deposition distribution on the left-hand wall for the above cases in order to determine whether or not the predicted deposition pattern matched the test results. This study tested three grid resolutions (534,671, 927,630, and 2,304,332) for the test chamber and found that a grid number of 927,630 provided grid-independent results. After the near-wall turbulence kinetic energy modification and a particle number independence test, this investigation evenly released 0.66 million particles with a certain diameter and tracked their trajectories. Next, the local particle deposition velocity distribution was calculated using Eq. (6). The particle calculations were repeated for different particle sizes ranging from 0.8 to 10 μm. The local particle deposition velocity for $PM_{2.5}$ and PM_{10} was then calculated as a weighted average according to the size distribution shown in Figure 6. Finally, the distribution of particle accumulation on the measured area was calculated using Eq. (7).

Figure 7 compares the particle deposition patterns obtained from the experiments and CFD calculations for both $PM_{2.5}$ and PM_{10}. In the photographs taken in the experiments, the bright areas represent the deposited particles, and the black areas are the background. For both $PM_{2.5}$ and PM_{10}, almost no particle deposition can be seen on the wall area under the linear diffuser. On the other hand, particle deposition under the bars of the multi-slot diffuser can be clearly observed. The proposed model predicted a similar distribution of particle accumulation. The calculated particle accumulation under the linear diffuser was less than 0.1 g/m^2, which would be almost invisible. However, under the bars of the multi-slot diffuser, a large portion of the predicted particle accumulation was greater than 1.0 g/m^2, which means that the stains would

be easily observable [54]. In general, the predicted distribution of particle deposition around the diffusers agreed well with that obtained from the chamber tests.

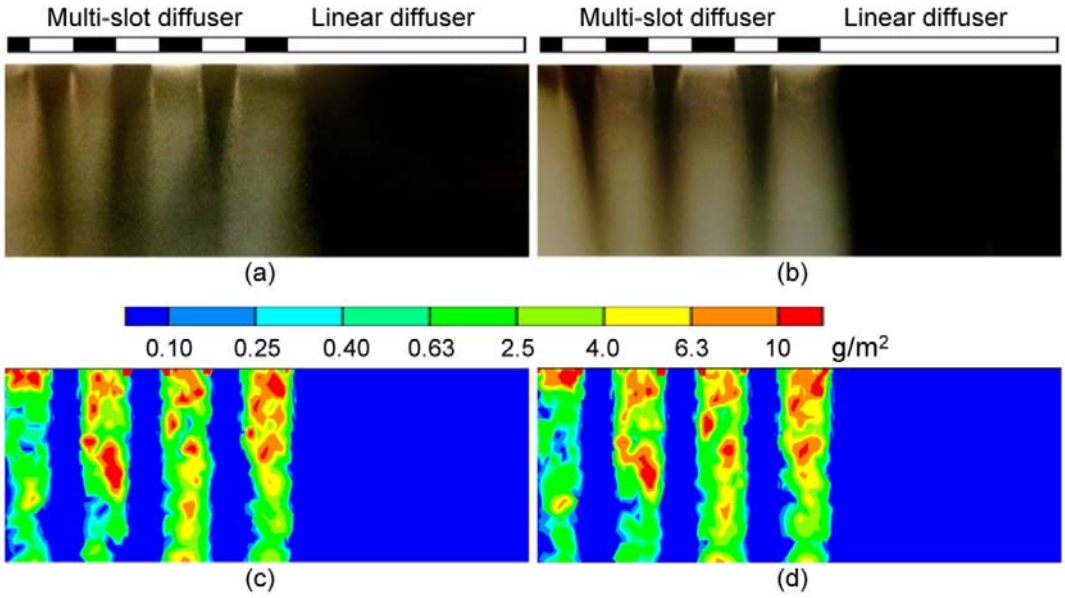

Figure 7. Particle deposition patterns on the left-hand wall under the multi-slot diffuser and the linear diffuser: (a) experiment for $PM_{2.5}$, (b) experiment for PM_{10}, (c) calculation for $PM_{2.5}$, and (d) calculation for PM_{10}.

There are several reasons for the formation of such a deposition distribution. In this case, the effects of Brownian diffusion and gravitational settling were limited on the left-hand wall under the diffusers. In general, when turbulent diffusion is the dominating deposition mechanism, the amount of deposited particles depends on the "competition" between two factors. One factor is the turbulent diffusion toward the wall, and the other is the particle movement with the mean flow parallel to the wall. The air near the left-hand wall had much greater turbulent fluctuating velocities than other locations because of the jets from the diffuser. This greater velocity caused stronger turbulent diffusion toward the wall. At the locations under the bars of the multi-slot diffuser, air recirculation occurred between the supply air jets, where the mean velocity magnitude was much smaller than the jets. Stronger turbulent diffusion toward the wall with weak particle movement parallel to the wall led to a high possibility of particle deposition at these locations. Nevertheless, at the locations under the linear diffuser and the openings of the multi-slot diffuser, particle movement with the mean flow parallel to the wall was very strong because of the high velocity jets. Although the turbulent diffusion at these locations was also strong, it could not "compete" with the even stronger particle movement with the jets. In other words, the particles were blown away by the strong jets before they had a chance to deposit on the wall at these locations. Thus, the particle deposition under the linear diffuser and the openings of the multi-slot diffuser was minimal. In summary, to prevent enhanced particle deposition around a multi-slot diffuser, measures should be taken to reduce the turbulent diffusion in the regions between supply air jets.

Figure 8 compares the particle deposition patterns obtained from the experiments and CFD calculations for both $PM_{2.5}$ and PM_{10}, for the multi-slot diffuser that supplied air at an angle of

45°. In the experimental data, no clear pattern can be observed on the wall area under the diffuser for either $PM_{2.5}$ or PM_{10}. The predicted particle deposition distribution did not exhibit a clear pattern either. When the experimental results in Figures 8 and 7 are compared, it can be seen that significantly fewer particles were deposited in this case than in the previous case. The proposed model correctly predicted the considerably lower particle accumulation. Therefore, this case provided further qualitative confirmation of the validity of the proposed model for predicting the distribution of particle deposition around a multi-slot diffuser.

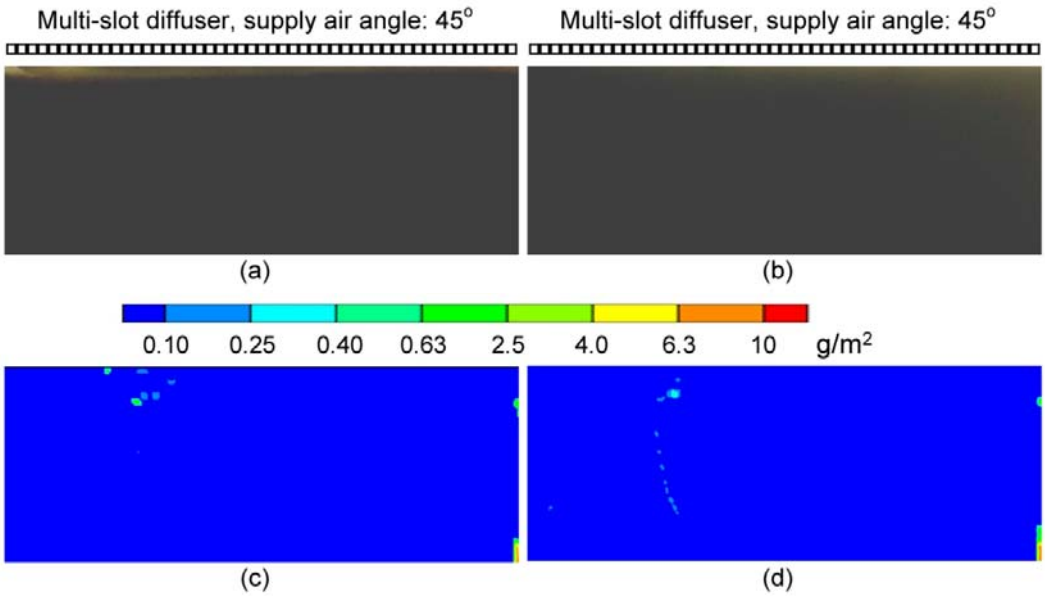

Figure 8. Comparison of experimentally determined and predicted particle deposition patterns on the left-hand wall under a slot diffuser supplying air at an angle of 45° for (a) $PM_{2.5}$ and (b) PM_{10}.

4. Parametric study

Using the validated model, this study conducted a parametric study to numerically investigate the effects of slot setting, supply air angle, and temperature differential on particle deposition around a multi-slot diffuser.

4.1 Case description

This study used a test chamber, as shown in Figure 5(a), with different parameter settings to examine their effects on particle deposition on the left-hand wall under the multi-slot diffuser. The studied cases with their slot settings, supply air angles, and temperature differentials are listed in Table 1. Note that the supply airflow rate was identical for all the cases because this parameter was pre-determined according to the heating/cooling load. Under the same supply airflow rate, different slot settings can result in different supply air velocities. Consequently, the spatial particle concentration near the diffuser as well as the deposition pattern may be altered. Four different slot settings, Cases 1 through 4, were compared in this study as shown in Table 1. For Cases 1 and 2, the supply air velocities were the same, but the lengths of the bars between openings were 5 and 2.5 cm, respectively. For Cases 1, 3, and 4, the area ratio of openings to bars was 1, 4, and 0.25, respectively, which resulted in different supply air

velocities with the same airflow rate. This study further designed Cases 1, 5, 6, and 7 to test the influence of supply air angle on particle deposition on the wall. The supply air angle was set at 0, 30, 45, and 60°, respectively, in these cases. Cases 1 through 7 were under isothermal conditions, while Cases 8 and 9 were designed to include the impact of temperature differentials. Particles can be driven from the high-temperature side to the low-temperature side by the thermophoretic force. For Case 8, under winter conditions, the supply air temperature was set at 32 °C according to the ASHRAE standard-55 [58], and the temperature of the left-hand wall was set at 5 °C to simulate a poorly insulated exterior wall. For Case 9, under summer conditions, the supply air temperature was set at 14 °C, and the temperature of the left-hand wall was set at 35 °C. Comparing Cases 8 and 9 with Case 1 allowed the impact of thermophoresis on particle deposition around a multi-slot diffuser to be investigated. Since most enhanced soiling problems occur within a few weeks to a few months after the system is under operation, this study calculated the distribution of $PM_{2.5}$ accumulation over a month for all the cases. The indoor $PM_{2.5}$ concentration was set at 14.2 μg/m^3, which is the median value for non-smoking homes in the U.S. as reported by Meng et al. [59].

Table 1. Case setup for the parametric study.

Case No.	Slot setting[1]	Supply air velocity (m/s)	Supply air angle (°)	Temperature differential[2] (°C)
1		1.99	0	0
2		1.99	0	0
3		0.995	0	0
4		3.98	0	0
5		1.99	30	0
6		1.99	45	0
7		1.99	60	0
8		1.99	0	27
9		1.99	0	–21

[1]The white areas represent the openings, while the black areas represent the bars between the openings.

[2]Temperature differential between the supply air and left-hand wall.

4.2 Results

Figure 9 shows the distribution of $PM_{2.5}$ accumulation on the left-hand wall over a period of a month under different slot settings. The wall area shown in the figure was directly under the diffuser, with the z-coordinate ranging from 1.5 to 2.2 m. A comparison of Cases 1 and 2 shows that the bar length in the multi-slot diffuser could affect the particle accumulation distribution. However, the amounts of accumulated particles on this wall area for Cases 1 and 2 were 0.040 and 0.035 g, respectively, which were on the same order of magnitude. A comparison of Cases 1, 3, and 4 shows that the area ratio of openings to bars was 0.25, 1, and 4, respectively. These values corresponded to supply air velocities of 3.98, 1.99, and 0.995 m/s, respectively. In the figure, it can be observed that a larger area ratio of openings to bars could significantly reduce the particle deposition on the wall. The amount of accumulated particles for Case 4 was the greatest (0.13 g), followed by Case 1 (0.040 g) and then Case 3 (0.0048 g). The results indicate that, with the same supply airflow rate, a lower supply air velocity reduced the particle

deposition on the wall around the multi-slot diffuser. This was because a lower supply air velocity would have resulted in lower turbulent fluctuating velocities, which reduced the turbulent diffusion toward the wall. When designing a multi-slot diffuser one should consider enlarging the area ratio of openings to bars in order to mitigate the soiling problem, once higher-priority design requirements have been met.

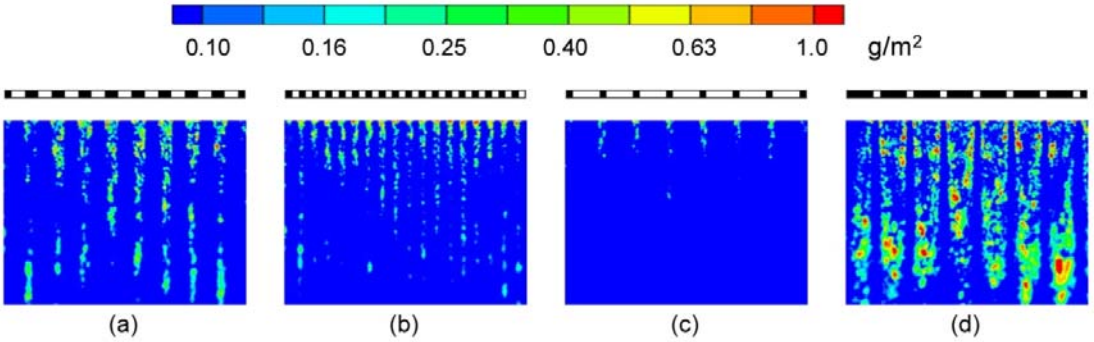

Figure 9. Distribution of $PM_{2.5}$ accumulation on the left-hand wall over a period of a month under different slot settings: (a) Case 1, (b) Case 2, (c) Case 3, and (d) Case 4.

Figure 10 compares the distributions of $PM_{2.5}$ accumulation on the left-hand wall over a period of a month under different supply air angles. A comparison of Cases 1 and 5 shows that when the angle was increased from 0 to 30°, less particle deposition occurred on the lower part of the wall. On the upper part of the wall near the multi-slot diffuser, however, the particle deposition was more pronounced. As a result, the total amount of accumulated particles on the wall area was greater in Case 5 (0.068 g) than in Case 1 (0.040 g). This was because the airflow pattern resulted in greater turbulent fluctuating velocities under the bars of the diffuser, which led to stronger turbulent diffusion toward the wall. When the supply air angle was larger than 45°, there was significantly less particle deposition on the wall. In Cases 6 and 7, the amounts of accumulated particles were reduced to 0.015 and 0.011 g, respectively. This was because the high-velocity jets were detached from the wall and did not produce high turbulent fluctuating velocities near the wall. Consequently, the corresponding turbulent diffusion toward the wall was significantly reduced. If a small angle between the air jet and the wall could be avoided in the design of a multi-slot diffuser, the soiling problem due to particle deposition on the wall might be resolved.

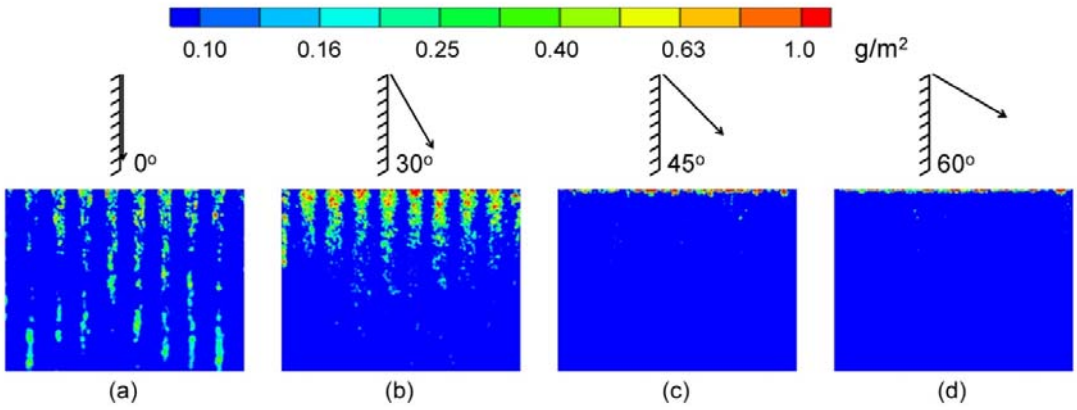

Figure 10. Distribution of $PM_{2.5}$ accumulation on the left-hand wall over a period of a month under different supply air angles: (a) Case 1, (b) Case 5, (c) Case 6, and (d) Case 7.

Figure 11 illustrates the distribution of $PM_{2.5}$ accumulation on the left-hand wall over a period of a month with temperature differentials of 0, 27, and -21 °C between the supply air and the left-hand wall. In general, the distributions of particle deposition were similar, and the amounts of particle accumulation were very close. In Case 8, which was under winter conditions, the temperature of the air was higher than that of the left-hand wall, and thus the particle deposition would have been enhanced by thermophoresis. However, the particle accumulation in Case 8 was only 1.1% higher than that in Case 1. In Case 9, which was under summer conditions, the particle deposition would have been reduced by thermophoresis. Nevertheless, the particle accumulation in Case 9 was only 1.4% less than in the isothermal case. Therefore, the impact of thermophoresis was almost negligible when compared with that of turbulent diffusion. This finding is consistent with the results of several other studies [24,28]. This conclusion may also be indirectly supported by the fact that soiling around diffusers commonly occurs in summer when central air-conditioning systems are operating. During this season, the supply air temperature should be lower than the wall temperature, which will result in less thermophoresis-driven particle deposition. Thus, the appearance of soiling around a diffuser in summer indicates that the problem is independent of thermophoresis.

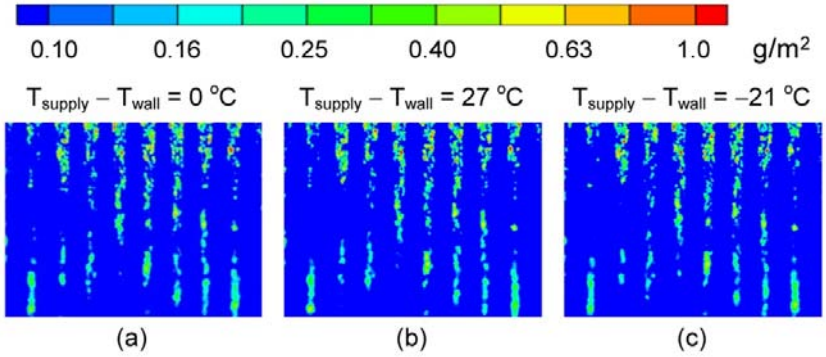

Figure 11. Distribution of $PM_{2.5}$ accumulation on the left-hand wall under the multi-slot diffuser over a period of a month under different temperature differentials between the supply air and the wall: (a) Case 1, (b) Case 8, and (c) Case 9.

5. Discussion

There are a number of limitations to the present study, beginning with the assumption of smooth surfaces. In an indoor environment, a rough surface could increase the overall particle deposition velocity by several times when compared with a smooth surface [60,61]. Since many indoor surfaces are considered to be rough, this study tended to under-estimate the deposition of particles. From the design perspective, such conservative predictions would still help designers to avoid potential soiling problems. Furthermore, although this study obtained qualitative information about deposition distribution by conducting chamber tests, quantitative data are still needed for further validation of the model. The cases with quantitative data in section 3.1 did not differentiate surfaces with different orientations and locations. The main reason was the difficulty in experimental design. The fluorescent particle experimental method

proposed by Lai and Nazaroff [14] may be used to obtain such quantitative data. In addition, although this study focused only on multi-slot diffusers, there are many other types of indoor diffusers, such as square, round, 4-way, swirl, and grille diffusers. The proposed model can be used as a tool to improve the design of these diffusers for the avoidance of soiling.

This study used a small chamber instead of a full-scale aircraft cabin or office to investigate the particle deposition on the surfaces near a multi-slot diffuser. That was because the method was developed mainly for assisting the engineers in the design of multi-slot diffusers to prevent enhanced soiling. The airflow characteristics near a diffuser should be mainly determined by the diffuser itself and the airflow rate. It means that the particle deposition on the surfaces near a diffuser should be independent from the size of the room. Therefore, in the design phase, using a small chamber should be sufficient to capture the characteristics of particle deposition on the surfaces near a diffuser. This strategy would significantly reduce the number of grid needed for the CFD calculations.

This study used particle accumulation, in g/m^2, to roughly estimate the visibility of deposited particles, as suggested by Holopainen et al. [54]. However, the actual visibility may also be influenced by other factors. One of these factors is the chemical composition and appearance of the airborne and deposited particles. For instance, black elemental carbon particles can absorb light that would usually be reflected by the walls, which makes the walls appear darker [62]. Also, the presence of SVOCs indoors was found to be correlated with the problem of enhanced soiling [10]. The condensation of organic materials on the particles may increase the visibility of the stains [30]. Furthermore, the larger particle size tends to induce more condensation of SVOCs, which may cause more observed blackening [30]. Clearly, the phenomenon of enhanced soiling around a diffuser is triggered by multiple factors. Further interdisciplinary research on this subject would provide a better understanding of this phenomenon.

6. Conclusions

This study proposed an SST k-ω model with a modified Lagrangian method to calculate the particle deposition on the surfaces around a multi-slot diffuser. The proposed model was validated by measured particle deposition rates from the literature and by the deposition patterns obtained from our chamber tests. This investigation then used the model to numerically investigate the effects of slot setting, supply air angle, and temperature differential on particle deposition around a multi-slot diffuser. The proposed model can be used in the design of multi-slot diffusers to prevent enhanced soiling on the wall due to particle deposition. Within the scope of this research, the following conclusions can be drawn:

(1) The proposed model can predict the particle deposition on the surfaces around a multi-slot diffuser reasonably well.

(2) With the same supply airflow rate, increasing the area ratio of openings to bars in a multi-slot diffuser can reduce the deposition of particles on the surrounding surfaces.

(3) Increasing the angle between the supply air jet and the wall to more than 45^o can significantly reduce the particle deposition around a multi-slot diffuser.

(4) The impact of thermophoresis on particle deposition on the surfaces around a multi-slot diffuser is negligible.

Acknowledgements
This research was partially sponsored by Key Project 15JCZDJC40900 of the Applied Basic and Frontier Technology Research Program, Tianjin Commission of Science and Technology, China, and the National Natural Science Foundation of China through Grant No. 51478302.

References
[1] Pope III, C. A., Burnett, R. T., Thun, M. J., Calle, E. E., Krewski, D., Ito, K., & Thurston, G. D. (2002). Lung cancer, cardiopulmonary mortality, and long-term exposure to fine particulate air pollution. Jama, 287(9), 1132-1141.
[2] Yu, O., Sheppard, L., Lumley, T., Koenig, J. Q., & Shapiro, G. G. (2000). Effects of ambient air pollution on symptoms of asthma in Seattle-area children enrolled in the CAMP study. Environmental Health Perspectives, 108(12), 1209.
[3] Pope III, C. A., Burnett, R. T., Thurston, G. D., Thun, M. J., Calle, E. E., Krewski, D., & Godleski, J. J. (2004). Cardiovascular mortality and long-term exposure to particulate air pollution epidemiological evidence of general pathophysiological pathways of disease. Circulation, 109(1), 71-77.
[4] Chen, C., & Zhao, B. (2011). Review of relationship between indoor and outdoor particles: I/O ratio, infiltration factor and penetration factor. Atmospheric Environment, 45(2), 275-288.
[5] Klepeis, N. E., Nelson, W. C., Ott, W. R., Robinson, J. P., Tsang, A. M., Switzer, P., Behar, J.V., Hern, S.C., & Engelmann, W. H. (2001). The National Human Activity Pattern Survey (NHAPS): A resource for assessing exposure to environmental pollutants. Journal of Exposure Analysis and Environmental Epidemiology, 11(3), 231-252.
[6] Chen, C., Zhao, B., & Weschler, C. J. (2012). Indoor exposure to "outdoor PM10": Assessing its influence on the relationship between PM10 and short-term mortality in US cities. Epidemiology, 23(6), 870-878.
[7] Lai, A. C. K. (2002). Particle deposition indoors: A review. Indoor Air, 12(4), 211-214.
[8] Nazaroff, W. W. (2004). Indoor particle dynamics. Indoor Air, 14(s7), 175-183.
[9] Cooper, D. W. (1986). Particulate contamination and microelectronics manufacturing: An introduction. Aerosol Science and Technology, 5(3), 287-299.
[10] Salthammer, T., Fauck, C., Schripp, T., Meinlschmidt, P., Willenborg, S., & Moriske, H. J. (2011). Effect of particle concentration and semi-volatile organic compounds on the phenomenon of "black magic dust" in dwellings. Building and Environment, 46(10), 1880-1890.
[11] Chao, C. Y. H., Wan, M. P., & Cheng, E. C. (2003). Penetration coefficient and deposition rate as a function of particle size in non-smoking naturally ventilated residences. Atmospheric Environment, 37(30), 4233-4241.
[12] Wallace, L. A., Emmerich, S. J., & Howard-Reed, C. (2004). Effect of central fans and in-duct filters on deposition rates of ultrafine and fine particles in an occupied townhouse. Atmospheric Environment, 38(3), 405-413.
[13] He, C., Morawska, L., & Gilbert, D. (2005). Particle deposition rates in residential houses. Atmospheric Environment, 39(21), 3891-3899.
[14] Lai, A. C. K., & Nazaroff, W. W. (2005). Supermicron particle deposition from turbulent flow onto vertical surfaces with varying roughness. Atmospheric Environment, 39, 4893-4900.
[15] El Hamdani, S., Limam, K., Abadie, M. O., & Bendou, A. (2008). Deposition of fine

particles on building internal surfaces. Atmospheric Environment, 42(39), 8893-8901.
[16] Hussein, T., Hruška, A., Dohányosová, P., Džumbová, L., Hemerka, J., Kulmala, M., & Smolík, J. (2009). Deposition rates on smooth surfaces and coagulation of aerosol particles inside a test chamber. Atmospheric Environment, 43(4), 905-914.
[17] Shi, S., Li, Y., & Zhao, B. (2014). Deposition velocity of fine and ultrafine particles onto manikin surfaces in indoor environment of different facial air speeds. Building and Environment, 81, 388-395.
[18] Lai, A. C. K., & Nazaroff, W. W. (2000). Modeling indoor particle deposition from turbulent flow onto smooth surfaces. Journal of Aerosol Science, 31(4), 463-476.
[19] Zhao, B., & Wu, J. (2007). Particle deposition in indoor environments: Analysis of influencing factors. Journal of Hazardous Materials, 147(1), 439-448.
[20] Zhao, B., Li, X., & Zhang, Z. (2004). Numerical study of particle deposition in two differently ventilated rooms. Indoor and Built Environment, 13(6), 443-451.
[21] Chen, F., Simon, C. M., & Lai, A. C. (2006). Modeling particle distribution and deposition in indoor environments with a new drift–flux model. Atmospheric Environment, 40(2), 357-367.
[22] Gao, N. P., & Niu, J. L. (2007). Modeling particle dispersion and deposition in indoor environments. Atmospheric Environment, 41(18), 3862-3876.
[23] Parker, S., Nally, J., Foat, T., & Preston, S. (2010). Refinement and testing of the drift-flux model for indoor aerosol dispersion and deposition modelling. Journal of Aerosol Science, 41(10), 921-934.
[24] Zhao, B., Chen, C., & Tan, Z. (2009). Modeling of ultrafine particle dispersion in indoor environments with an improved drift flux model. Journal of Aerosol Science, 40(1), 29-43.
[25] Abdolzadeh, M., Mehrabian, M. A., Zahedi, G., & Goharrizi, A. S. (2011). Effect of thermophoresis and other parameters on the particle deposition on a tilted surface. International Journal of Heat and Fluid Flow, 32(3), 670-679.
[26] Bouilly, J., Limam, K., Béghein, C., & Allard, F. (2005). Effect of ventilation strategies on particle decay rates indoors: An experimental and modelling study. Atmospheric Environment, 39(27), 4885-4892.
[27] Lai, A. C. K., & Chen, F. (2006). Modeling particle deposition and distribution in a chamber with a two-equation Reynolds-averaged Navier–Stokes model. Journal of Aerosol Science, 37(12), 1770-1780.
[28] Zhang, Z., & Chen, Q. (2009). Prediction of particle deposition onto indoor surfaces by CFD with a modified Lagrangian method. Atmospheric Environment, 43(2), 319-328.
[29] Wang, M., Lin, C. H., & Chen, Q. (2011). Determination of particle deposition in enclosed spaces by Detached Eddy Simulation with the Lagrangian method. Atmospheric Environment, 45(30), 5376-5384.
[30] Fittschen, U. E., Santen, M., Rehmers, A., Durukan, I., & Wesselmann, M. (2012). Indoor aerosol determination with respect to a soiling phenomenon in private residences. Environmental Science & Technology, 47(1), 608-615.
[31] Sundell, J., Levin, H., Nazaroff, W. W., Cain, W. S., Fisk, W. J., Grimsrud, D. T., Grimsrud, D.T., Gyntelberg, F., Li, Y., Persily, A.K., Pickering, A.C. & Samet, J. M. (2011). Ventilation rates and health: Multidisciplinary review of the scientific literature. Indoor Air, 21(3), 191-204.

[32] Chen, X., & Li, A. (2014). An experimental study on particle deposition above near-wall heat source. Building and Environment, 81, 139-149.
[33] Chen, X., Li, A., & Gao, R. (2014). Numerical investigation on particle deposition in a chamber with an attached-wall heat source. Indoor and Built Environment, 23(5), 640-652.
[34] Timmer, H., & Zeller, M. (2004). Particle deposition near ceiling induction outlets. International Journal of Refrigeration, 27(3), 248-254.
[35] Kloostra, L., and Aswegan, J. (2012). Smudging around air distribution diffusers. Air Conditioning, Heating & Refrigeration News, Extra Edition, December 03, 2012. (http://www.achrnews.com/articles/121501-smudging-around-air-distribution-diffusers)
[36] Richardson D. 2014. Duct dynasty: Why dirt streaking occurs around your supply vents. Air Conditioning, Heating & Refrigeration News, January 26, 2015. (http://www.achrnews.com/articles/128615-why-dirt-streaking-occurs-around-vents)
[37] Liu, W., Wen, J., Chao, J., Yin, W., Shen, C., Lai, D., Lin, C.H., Liu, J., Sun, H., & Chen, Q. (2012). Accurate and high-resolution boundary conditions and flow fields in the first-class cabin of an MD-82 commercial airliner. Atmospheric Environment, 56, 33-44.
[38] Li, J., Cao, X., Liu, J., Wang, C., & Zhang, Y. (2015). Global airflow field distribution in a cabin mock-up measured via large-scale 2D-PIV. Building and Environment, 93, 234-244.
[39] Cao, X., Li, J., Liu, J., & Yang, W. (2016). 2D-PIV measurement of isothermal air jets from a multi-slot diffuser in aircraft cabin environment. Building and Environment, 99, 44-58.
[40] Menter, F. R. (1994). Two-equation eddy-viscosity turbulence models for engineering applications. AIAA Journal, 32(8), 1598-1605.
[41] Shi, Z., Chen, J., & Chen, Q. (2015). On the turbulence models and turbulent Schmidt number in simulating stratified flows. Journal of Building Performance Simulation, 1-15.
[42] You, R., Chen, J., Shi, Z., Liu, W., Lin, C. H., Wei, D., & Chen, Q. (2016). Experimental and numerical study of airflow distribution in an aircraft cabin mock-up with a gasper on. Journal of Building Performance Simulation, DOI: 10.1080/19401493.2015.1126762.
[43] Hinds, W.C. (1999). Aerosol Technology: Properties, Behavior, and Measurement of Airborne Particles, 2nd edition. New York: Wiley.
[44] Zhao, B., Chen, C., Yang, X., & Lai, A. C. (2010). Comparison of three approaches to model particle penetration coefficient through a single straight crack in a building envelope. Aerosol Science and Technology, 44(6), 405-416.
[45] Matida, E. A., Nishino, K., & Torii, K. (2000). Statistical simulation of particle deposition on the wall from turbulent dispersed pipe flow. International Journal of Heat and Fluid Flow, 21(4), 389-402.
[46] Matida, E. A., Finlay, W. H., Lange, C. F., & Grgic, B. (2004). Improved numerical simulation of aerosol deposition in an idealized mouth–throat. Journal of Aerosol Science, 35(1), 1-19.
[47] Chao, C. Y. H., Wan, M. P., & Sze To, G. N. (2008). Transport and removal of expiratory droplets in hospital ward environment. Aerosol Science and Technology, 42(5), 377-394.
[48] Wang, Y., & James, P. W. (1999). On the effect of anisotropy on the turbulent dispersion and deposition of small particles. International Journal of Multiphase Flow, 25(3), 551-558.
[49] Kim, J., Moin, P., & Moser, R. (1987). Turbulence statistics in fully developed channel flow at low Reynolds number. Journal of Fluid Mechanics, 177, 133-166.
[50] He, C., & Ahmadi, G. (1999). Particle deposition in a nearly developed turbulent duct flow

with electrophoresis. Journal of Aerosol Science, 30(6), 739-758.
[51] NADCA. (1992). Mechanical Cleaning of Non-Porous Air Conveyance System Components, An Industry Standard Developed by the National Air Duct Cleaners Association. Washington, DC, NADCA, 1992-01.
[52] HVCA. (1998). Cleanliness of Ventilation Systems, Guide to Good Practice Cleanliness of Ventilation Systems. Heating and Ventilating Contractors Association, London, HVCA Publications, (TR/17).
[53] FiSIAQ. (2001). Classification of Indoor Climate, Construction, and Building Materials 2000. Finnish Society of Indoor Air Quality and Climate, Espoo, Finland.
[54] Holopainen, R., Narvanne, J., Pasanen, P., & Seppänen, O. (2002). A visual inspection method to evaluate cleanliness of newly installed air ducts. In Proceedings of the 9th International Conference on Indoor Air Quality and Climate, Indoor Air (pp. 682-687).
[55] ANSYS. (2014). ANSYS 16.0 Fluent Documentation. Canonsburg, PA.
[56] You, R., Cui, W., Chen, C., & Zhao, B. (2013). Measuring the short-term emission rates of particles in the "personal cloud" with different clothes and activity intensities in a sealed chamber. Aerosol and Air Quality Research, 13, 911-921.
[57] Bredell, J. R., Kröger, D. G., & Thiart, G. D. (2006). Numerical investigation of fan performance in a forced draft air-cooled steam condenser. Applied Thermal Engineering, 26(8), 846-852.
[58] ASHRAE, A.N.S.I. (2004). Standard 55-2004, Thermal environmental conditions for human occupancy. American Society of Heating, Refrigerating and Air-Conditioning Engineering, Atlanta, GA.
[59] Meng, Q. Y., Spector, D., Colome, S., & Turpin, B. (2009). Determinants of indoor and personal exposure to PM 2.5 of indoor and outdoor origin during the RIOPA study. Atmospheric Environment, 43(36), 5750-5758.
[60] Abadie, M., Limam, K., & Allard, F. (2001). Indoor particle pollution: Effect of wall textures on particle deposition. Building and Environment, 36(7), 821-827.
[61] Lai, A. C., Byrne, M. A., & Goddard, A. J. (2002). Experimental studies of the effect of rough surfaces and air speed on aerosol deposition in a test chamber. Aerosol Science & Technology, 36(10), 973-982.
[62] Bellan, L. M., Salmon, L. G., & Cass, G. R. (2000). A study on the human ability to detect soot deposition onto works of art. Environmental Science & Technology, 34(10), 1946-1952.